Weak entanglement improves quantum communication using only product measurements

Amélie Piveteau, Alastair A. Abbott, Sadiq Muhammad, Mohamed Bourennane, Armin Tavakoli

Weak entanglement improves quantum communication using only product measurements

Amélie Piveteau,[1] Alastair A. Abbott,[2] Sadiq Muhammad,[1] Mohamed Bourennane,[1] and Armin Tavakoli[3,*]

[1] *Department of Physics, Stockholm University, SE-106 91 Stockholm, Sweden*
[2] *Univ. Grenoble Alpes, Inria, 38000 Grenoble, France*
[3] *Physics Department, Lund University, Box 118, SE-221 00 Lund, Sweden*

(Received 17 March 2023; revised 30 January 2024; accepted 5 February 2024; published 25 March 2024)

We show that weakly entangled states can improve communication over a qubit channel using only separate, interference-free, measurements of individual photons. We introduce a communication task corresponding to the cryptographic primitive known as secret sharing and show that all steerable two-qubit isotropic states provide a quantum advantage in the success rate using only product measurements. Furthermore, we show that such measurements can even reveal communication advantages from noisy partially entangled states that admit no quantum steering. We then go further and consider a stochastic variant of secret sharing based on more-sophisticated, yet standard, partial Bell-state analyzers, and show that this reveals advantages also for a range of unsteerable isotropic states. By preparing polarization qubits in unsteerable states, we experimentally demonstrate increased success rates of both secret-sharing tasks beyond the best entanglement-unassisted qubit protocol. Our results reveal the capability of simple and scalable measurements in entanglement-assisted quantum communication to overcome large amounts of noise.

DOI: 10.1103/PhysRevApplied.21.034053

I. INTRODUCTION

Entanglement is well known to be a crucial resource for quantum communication applications. However, not all forms of entanglement are always useful. For instance, while entanglement that is strong enough to generate nonlocality has been found to improve noiseless classical communication beyond its conventional limitations (see, e.g., Refs. [1–6]), weaker entangled states that cannot violate any Bell inequality do not have that ability [7]. In contrast, if the system communicated is itself quantum, e.g., a qubit instead of a bit, then some weaker forms of entanglement also become useful. This can be seen in the dense-coding protocol [8], where a maximally entangled state, $|\phi^+\rangle = (|00\rangle + |11\rangle)/\sqrt{2}$, is used to allow a qubit message to transmit two bits instead of one bit. When the state is noisy, the isotropic state

$$\rho_v = v|\phi^+\rangle\langle\phi^+| + \frac{1-v}{4}\mathbb{1}, \tag{1}$$

where $v \in [0,1]$ is the visibility, achieves an advantage over an unassisted-qubit message whenever $v > 1/3$ [9,10]. This coincides with the visibility at which the state becomes separable, $v_{\text{sep}} = 1/3$, and it is considerably lower than the critical visibility for quantum steering, $v_{\text{unsteer}} = 1/2$ [11,12], and far below the even-higher visibility needed for Bell nonlocality [13].

However, to harness the dense-coding advantage, one must measure in the Bell basis $\{\Phi^+, \Phi^-, \Psi^+, \Psi^-\}$, where $\Phi^\pm = |\phi^\pm\rangle\langle\phi^\pm|$ and $\Psi^\pm = |\psi^\pm\rangle\langle\psi^\pm|$ are the projectors onto the states $|\phi^\pm\rangle = (|00\rangle \pm |11\rangle)/\sqrt{2}$ and $|\psi^\pm\rangle = (|01\rangle \pm |10\rangle)/\sqrt{2}$. In optical systems, it is impossible to implement a linear-optics Bell-basis measurement on separate photons without the use of auxiliary photons [14]. While dense-coding experiments have been reported [15–19], implementation of the Bell basis is not expected to be scalable in optical systems soon. Nevertheless, it was recently found that entanglement can yield advantages in one-shot quantum communication scenarios by use of much-more-limited, yet much-less-experimentally-demanding, optical measurements that are compatible with passive linear optics or even just separate single-photon

*armin.tavakoli@teorfys.lu.se

measurements [20]. However, the schemes considered thus far come with greater requirements on the quality of entanglement, in particular needing states that violate a Bell inequality.

Here we show that the simplest optical measurements are sufficient to reveal communication advantages from highly noisy entangled states. To this end, we introduce a version of secret sharing. In secret sharing, a secret is distributed between two parties in such a way that they must cooperate to reconstruct it [21,22]. This is of considerable interest for quantum cryptography. Previous protocols achieved secret sharing in a device-dependent way, i.e., by assuming that devices perform specific operations (see e.g., Refs. [23–27]). In contrast, our protocols are semi-device-independent, in the sense that all operations are uncharacterized up to the assumption that they act on qubit systems. We prove that for our secret-sharing task every steerable isotropic state enables an advantage over unassisted qubits using only product measurements on separate photons. Furthermore, we also identify unsteerable states for which an advantage is possible with such measurements. In addition, we prove that, at the cost of using somewhat-more-sophisticated measurements, namely, partial Bell-state analyzers, which require optical interference but are still feasible with standard passive linear optics [28, 29], it is possible to reveal advantages from unsteerable instances of the isotropic state. For this, we use a stochastic modification of the original secret-sharing task. Using polarization qubits generated via spontaneous parametric down-conversion (SPDC), we use both a maximally entangled state to experimentally demonstrate optimal secret-sharing protocols and unsteerable states to outperform the best-possible entanglement-unassisted-qubit protocols using both product measurements and partial Bell-state analyzers.

II. DETERMINISTIC SECRET SHARING

Alice wishes to generate a random secret bit $a \in \{0,1\}$ that is shared with Bob and Charlie in such a way that they individually have no knowledge of a but can learn its value if they cooperate. To this end, we consider the scenario illustrated in Fig. 1. Bob and Charlie each privately select two uniformly random bits $x \equiv (x_0, x_1) \in \{0,1\}^2$ and $y \equiv (y_0, y_1) \in \{0,1\}^2$, respectively, and each communicates a message to Alice. Alice privately selects a binary input $z \in \{0,1\}$ and accordingly decodes the two incoming messages into an output $a \in \{0,1\}$. Here, z, which is later announced publicly, determines which bits of Bob and Charlie hold the shared secret: the success condition is $a = x_z \oplus y_z$. The average success probability of secret sharing becomes

$$\mathcal{S} = \frac{1}{32}\sum_{x,y,z} p(a = x_z \oplus y_z | x, y, z). \tag{2}$$

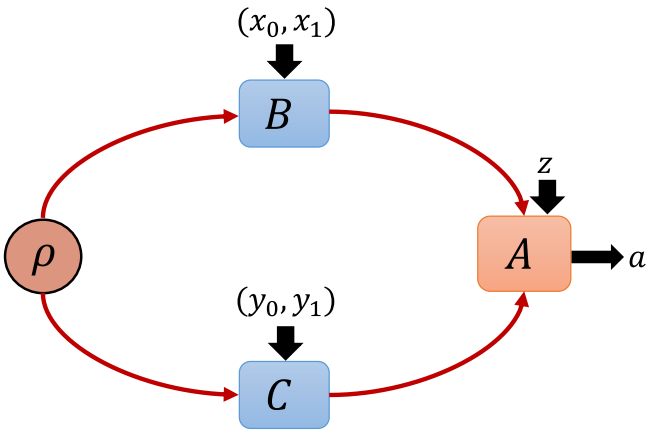

FIG. 1. Secret-sharing scenario. Bob (B) and Charlie (C) select private inputs and perform separate transformations on a shared two-qubit entangled state. They relay their respective output qubits to Alice (A), who measures them. Her output is the secret and her input determines how it can be reconstructed collectively by Bob and Charlie.

Naturally, the parties must have some physical limitations. In a purely classical scheme, Bob and Charlie would share only a classical random variable and they would individually send Alice classical messages in the form of a bit. Alice would use a decoding function to decide her output on the basis of her input. However, our main focus is on quantum protocols. On the one hand, we are interested in the situation in which Bob and Charlie share no prior entanglement and simply send messages encoded in qubit states β_x and γ_y, respectively, while Alice can decode the messages using a general quantum measurement $\{M_{a|z}\}_a$. The observed correlations are then given by $p_{\text{qubit}}(a|x,y,z) = \text{tr}\left[(\beta_x \otimes \gamma_y) M_{a|z}\right]$. On the other hand, we also consider the situation illustrated in Fig. 1, where Bob and Charlie may additionally share a two-qubit entangled state ρ and then encode their qubit messages through local quantum channels Λ_x^B and Λ_y^C, respectively. In this entanglement-assisted case, the correlations are given by $p_{\text{EAQ}}(a|x,y,z) = \text{tr}\left[\left(\Lambda_x^B \otimes \Lambda_y^C(\rho)\right) M_{a|z}\right]$. We now show that there exists an entanglement-assisted quantum protocol that achieves a perfect secret-sharing rate while requiring only separate measurements of the incoming quantum messages.

III. IDEAL ENTANGLEMENT-ASSISTED AND UNASSISTED PROTOCOLS

Consider a maximally entangled state $\rho = |\phi^+\rangle\langle\phi^+|$ and let Bob's and Charlie's local channels correspond to implementation of the four unitaries $U_x^B = \sigma_X^{x_0}\sigma_Z^{x_1}$ and $U_y^C = \sigma_X^{y_0}\sigma_Z^{y_1}$, respectively, where σ_X and σ_Z are the Pauli bit-flip and phase-flip operators. This means that the two-qubit state arriving at Alice is one of the four Bell states. When

$z = 0$, Alice measures $\sigma_Z \otimes \sigma_Z$, i.e., she discriminates the states $|\phi^{\pm}\rangle$ from the states $|\psi^{\pm}\rangle$. When $z = 1$, she measures $\sigma_X \otimes \sigma_X$, i.e., she discriminates the states $|\phi^{+}\rangle$ and $|\psi^{+}\rangle$ from the states $|\phi^{-}\rangle$ and $|\psi^{-}\rangle$. This gives $\mathcal{S} = 1$.

In contrast, in the scenario when entanglement is absent, it is no longer possible to succeed deterministically. We have determined the maximum value of $\mathcal{S}$ achievable with entanglement-unassisted qubits and general measurements for Alice. This is achieved with use of a straightforward modification of a hierarchy of semidefinite programs for bounding dimensionally restricted quantum correlation [30]. To obtain sufficiently tight upper bounds on $\mathcal{S}_{\text{qubit}}$, we have considered terms appearing in the first three levels of this hierarchy [31]. Up to solver precision, we obtain the upper bound $\mathcal{S}_{\text{qubit}} \leq 3/4$. This bound holds even if all three parties share some preagreed classical randomness.

A simple classical strategy can saturate $\mathcal{S}_{\text{qubit}}$, thus showing both that the bound is tight and that there exists no quantum-over-classical advantage without use of entanglement. To this end, consider that Bob and Charlie send x_0 and y_0, respectively, to Alice. When $z = 0$, she correctly outputs $a = x_0 \oplus y_0$, and when $z = 1$, she chooses a at random. This leads to $S_{\text{classical}} = 3/4$. We conclude that any value in the range $3/4 < \mathcal{S} \leq 1$ implies an advantage over both the best classical protocol and the best entanglement-unassisted quantum protocol, and hence is powered by the consumption of entanglement.

IV. ADVANTAGE FROM NOISY ENTANGLEMENT

If, in the above-described ideal entanglement-assisted protocol, we substitute the maximally entangled state for the isotropic state (1), we find that $\mathcal{S} = (1 + v)/2$. Hence, when $v > 1/2 = v_{\text{unsteer}}$, product measurements reveal an entanglement-based advantage in the task. We conclude that every steerable isotropic state is a communication resource under product measurements. Furthermore, while unsteerable isotropic states do not provide an advantage, there exist other unsteerable states that are useful in the task. To this end, consider the states $\rho_v^{\theta} = v|\phi_{\theta}^{+}\rangle\langle\phi_{\theta}^{+}| + (1 - v)/(4)\mathbb{1}$, where $v \in [0, 1]$ and $|\phi_{\theta}^{+}\rangle = \cos\theta|00\rangle + \sin\theta|11\rangle$ is a pure partially entangled state for $\theta \in (0, \pi/4]$. In the work reported in Ref. [32], local hidden state models were computed for ρ_v^{θ}. A particularly sizable advantage is found at $\theta_* = 0.2356$, for which the state is unsteerable when $v \lesssim 0.7325$ but achieves a secret-sharing success rate $\mathcal{S} > \mathcal{S}_{\text{qubit}}$ whenever $v \gtrsim 0.6878$. Hence, a significant amount of additional noise can be added to the unsteerable state before it ceases to generate a communication advantage under product measurements. Note also that applying the protocol to an arbitrary pure entangled state $|\phi_{\theta}^{+}\rangle$, we obtain $\mathcal{S} = (3 + \sin(2\theta))/4$, which exceeds the entanglement-unassisted limit if and only if the state is entangled.

V. STOCHASTIC SECRET SHARING

We have seen that advantages in secret sharing can be propelled by all steerable isotropic states when product measurements are used. Now we see that advantages can be obtained even with unsteerable isotropic states, at the cost of switching from product measurements to standard, linear-optics, partial Bell-state analyzers. To this end, we consider such measurements in a stochastic version of our secret-sharing task.

Consider again the scenario in Fig. 1 but now let Alice have three possible outcomes $a \in \{0, 1, \perp\}$, where $a \in \{0, 1\}$ corresponds to the secret bit stored in $x_{\bar{z}} \oplus y_{\bar{z}}$, where $\bar{z} = z \oplus 1$, and $a = \perp$ is associated with a control parameter that indicates that the round is not used for secret sharing. We define that a round should be used for secret sharing exclusively when $x_z \oplus y_z = 1$. Hence, the average success rate of secret sharing in the relevant rounds becomes

$$\mathcal{R}_{\text{secret}} = \frac{1}{16}\sum_{z}\sum_{x_z \oplus y_z = 1} p(a = x_{\bar{z}} \oplus y_{\bar{z}}|x, y, z), \quad (3)$$

whereas the average probability of correctly identifying a round not used for secret sharing $\mathcal{R}_{\text{control}}$ is $1/16\sum_z\sum_{x_z \oplus y_z = 0} p(a = \perp |x, y, z)$. This serves as a control parameter.

We are now interested in determining the largest value of $\mathcal{R}_{\text{secret}}$ for a given value of the control parameter. Note that an ideal protocol would achieve perfect secret sharing in all relevant rounds and perfectly identify all non-secret-sharing rounds, i.e., $\mathcal{R}_{\text{secret}} = \mathcal{R}_{\text{control}} = 1$. This is possible with entanglement: Bob and Charlie perform the same unitaries as before and Alice does a three-outcome measurement corresponding to a projection onto $\{\Psi^{+}, \Psi^{-}, \Phi^{+} + \Phi^{-}\}$ for $z = 0$ and onto $\{\Phi^{-}, \Psi^{-}, \Phi^{+} + \Psi^{+}\}$ for $z = 1$. These measurements may be seen as partial Bell-state analyzers, resolving two of the four Bell states, as compatible with passive linear optics [33].

In contrast, in the scenario when entanglement is absent, the trade-off between $\mathcal{R}_{\text{secret}}$ and $\mathcal{R}_{\text{control}}$ is nontrivial. Numerical exploration suggests that it is characterized by $\mathcal{R} = (1/2)\mathcal{R}_{\text{secret}} + (1/2)\mathcal{R}_{\text{control}} \leq 5/8$ with $\mathcal{R}_{\text{control}} \leq 3/4$. Using symmetries [34] to make the problem more tractable, we used semidefinite relaxations [35] to prove the upper bound of $5/8$ up to solver precision. As in the deterministic case, this bound can be saturated classically: Bob and Charlie relay the bits x_0 and y_0, respectively, to Alice. If $z = 1$, she outputs $a = x_0 \oplus y_0$. If $z = 0$, Alice outputs $a = \perp$ if $x_0 \oplus y_0 = 0$ and $a = 0$ otherwise. This gives $\mathcal{R}_{\text{secret}} = 3/4$ and $\mathcal{R}_{\text{control}} = 1/2$, thus saturating the entanglement-unassisted bound.

If the above-described entanglement-assisted protocol is performed with the isotropic state (1), we find that $\mathcal{R} = (3 + 5v)/8$. Thus, we observe an advantage ascribed to entanglement whenever $\mathcal{R} > 5/8$, which occurs whenever

$v > 2/5$. Consequently, when $v \in (2/5, 1/2]$, the isotropic state is both unsteerable and a communication resource with the decoding resources used.

VI. EXPERIMENT

We report here on experimental implementations of the deterministic and stochastic secret-sharing protocols. We implement both ideal quantum protocols using maximally entangled states encoded in the polarization of photons and protocols using weakly entangled, unsteerable, states. We begin by presenting the deterministic secret-sharing experiment using partially entangled states ρ_v^θ, before explaining how this is modified for the stochastic protocol using the simpler isotropic states ρ_v.

To generate the entangled states, ultraviolet light centered at a wavelength of 390 nm is focused onto two 2-mm-thick β-barium borate nonlinear crystals placed in an interferometric configuration to produce photon pairs emitted into two spatial modes (a) and (b) through the second-order degenerate type-I SPDC process. The spectral and temporal distinguishability between the down-converted photons is carefully removed by their passage through narrow-bandwidth interference filters and quartz wedges, respectively (see Fig. 2). For the deterministic secret-sharing protocol, we prepare the pure partially entangled state $|\phi_\theta^+\rangle = \cos\theta|HH\rangle + \sin\theta|VV\rangle$ by setting the polarization of the pump laser ($\cos\theta|H\rangle + \sin\theta|V\rangle$), where H and V are, respectively, the horizontal and vertical photonic polarization modes used to encode the basis states in the standard way as $|0\rangle := |H\rangle$ and $|1\rangle := |V\rangle$. We then prepare a depolarization ρ_v^θ of the state $|\phi_\theta^+\rangle = \cos\theta|HH\rangle + \sin\theta|VV\rangle$. To achieve the mixture with the maximally mixed state, we randomly transform, with probability $1 - v$, the pure partially entangled state into one of these four orthogonal states: $|\phi_\theta^+\rangle$, $|\phi_\theta^-\rangle = \sin\theta|HH\rangle - \cos\theta|VV\rangle$, $|\psi_\theta^+\rangle = \cos\theta|HV\rangle + \sin\theta|VH\rangle$, and $|\psi_\theta^-\rangle = \sin\theta|HV\rangle - \cos\theta|VH\rangle$. These transformations were experimentally realized by a motorized rotation of two half-wave plates (HWPs) and a phase shifter (PS); see Fig. 2. Details and experimental settings are provided in Appendix B. Alice performs product measurements in the H-V and diagonal bases using two HWPs placed before the input of two polarizing beam splitters (PBSs) distributed on each of the two modes (a) and (b); see box I in Fig. 2.

Bob's and Charlie's transformations U_x^B and U_y^C, respectively, are performed with use of two HWPs and a PS to change the relative phase between the two modes (a) and (b) (see Fig. 2 and Appendix B for the settings).

We chose visibility $v = 0.72$ (with $\theta = \theta_* = 0.2356$), for which the ideal state $\rho_v^{\theta_*}$ is unsteerable. Performing state tomography, we obtain a state fidelity of 0.9965 ± 0.0007 (see Appendix E), and we verified that the experimentally realized state is indeed unsteerable. In the implementation of the protocol, the two-photon-coincidence rate

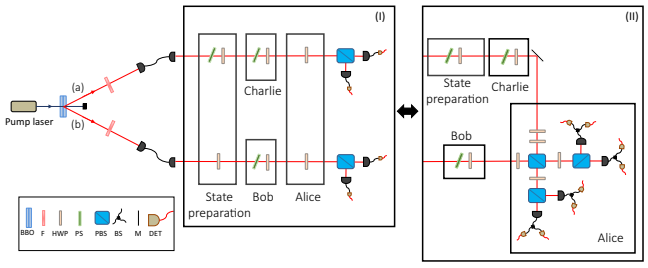

FIG. 2. Experimental setup. Entangled photon pairs in spatial modes (a) and (b) are generated through the SPDC process. For the deterministic secret-sharing experiment (box I), entangled photon pairs are generated in the same way but with a different ratio between the two modes. Isotropic states are prepared by random transformation of the maximally entangled $|\phi^+\rangle$ state into one of three other Bell states using two HWPs and a PS. The unitaries of Bob and Charlie are implemented with use of HWPs and PSs. Alice's projective measurements are implemented with the use of HWPs and PBSs and then detected by single-photon detectors (DETs). For the stochastic secret-sharing experiment (box II), isotropic states are prepared by random transformation of the maximally entangled $|\phi^+\rangle$ state into one of the other Bell states using one HWP and one PS. The unitaries of Bob and Charlie are implemented with use of HWPs and PSs. Alice's partial Bell-state measurements are implemented with the use of HWPs, PBSs, and beam splitters (BSs) and then detected by single-photon detectors. BBO, β-barium borate; F, filter, M, mirror.

was one per second. The total number of events recorded is approximately 8×10^5, leading to $\mathcal{S} = 0.757 \pm 0.001$, which is significantly above the entanglement-unassisted limit, $\mathcal{S} = 3/4$ (see Appendix D). We also performed the protocol using the pure state $|\phi_{\theta_*}^+\rangle = \cos\theta_*|HH\rangle + \sin\theta_*|VV\rangle$, with a total of 7×10^7 two-photon-coincidence events. We measured the state fidelity to be 0.990 ± 0.0001 and found a success probability $\mathcal{S}$ of 0.8519 ± 0.0002, which can be compared which the theoretical prediction of $\mathcal{S} \approx 0.8635$.

For the stochastic secret-sharing protocol, we prepared the maximally entangled state $|\phi^+\rangle$ and isotropic states ρ_v in a similar way (recalling that $|\phi^+\rangle = |\phi_{\pi/4}^+\rangle$). In this case the mixing with white noise, obtained by our randomly transforming, with probability $1 - v$, $|\phi^+\rangle$ into one of the four Bell states $|\phi^\pm\rangle, |\psi^\pm\rangle$ is simplified, and was realized by a motorized rotation of one HWP and a PS placed on the mode (a); see Fig. 2. Bob's and Charlie's transformations remain the same as in the deterministic secret-sharing protocol.

The polarization measurements are performed with the use of HWPs and PBSs, beam splitters placed at the two output ports of the PBSs, and then single-photon detectors (actively quenched Si avalanche photodiodes). The partial Bell-state analyzer (Fig. 2, box II) is implemented through two-photon interference with PBSs and HWPs

set at 22.5°. The two-photon Hong-Ou-Mandel dip visibility is $(99.2 \pm 0.6)\%$, where the substantial statistical error is due to the low two-photon-coincidence rate used in the experiment (one per second) and a measurement time of 2400 s per point (see Appendix H). To switch from a Bell-state measurement discriminating between $\{\Psi^+, \Psi^-, \Phi^+ + \Phi^-\}$ and $\{\Phi^-, \Psi^-, \Phi^+ + \Psi^+\}$, Alice uses three HWPs placed before the first PBS (see Appendix F for the HWP settings). All single-detection events were registered with a VHDL-programmed multichannel coincidence logic unit, with a time coincidence window of 1.7 ns.

To perform state tomography of isotropic states ρ_v for different values of v, we performed tomography of the four Bell states generated in the randomization procedure. Measurements were made at a rate of one two-photon coincidence per second over 1400 s for each of the nine settings needed to perform the state tomography for each Bell state. These results were then recombined *a posteriori* at different ratios to establish the density matrices ρ_v. We considered the reconstructed states ρ_v for $v = 0.4$ to $v = 0.5$, with a step size of 0.01, corresponding to the resourceful but unsteerable range. Naturally, the reconstructed density matrices are not exactly isotropic states. To ensure the unsteerability of the experimentally realized states, we used the linear-programming method in Ref. [36], which allows one to obtain a certificate of unsteerability for an arbitrary two-qubit state. We chose to proceed during the experiment with $v = 0.47$, as this represented a good balance between being below the steering threshold of $v_{\text{unsteer}} = 1/2$ and allowing good-enough statistics to show a significant quantum advantage (see Appendix A). The fidelity of the reconstructed state with the target isotropic state for $v = 0.47$ is 0.9983 ± 0.0004. Detailed tomography results for the density matrices, the state fidelities, and the certificates of unsteerability are presented in Appendix I.

The protocol was then performed with the isotropic state at $v = 0.47$ with the noise added by our randomly changing the Bell state between each two-photon coincidence while maintaining the necessary ratio between these states. To obtain at most one event per change of Bell state and thus ensure the randomness and therefore unpredictability of each event, we chose to work at a rate of one two-photon-detection coincidence per second. The effective measurement time per setting was 2.8 h. We obtained a success probability $\mathcal{R}$ of 0.6524 ± 0.0004, which significantly goes beyond the theoretical entanglement-unassisted limit of $\mathcal{R}_{\text{qubit}} \leq 5/8$, hence showing an advantage from unsteerable states (see Appendix G).

The same experiment was also performed for a maximally entangled state $|\phi^+\rangle$, i.e., without any randomization over Bell states. This increased the rate to 800 two-photon-detection coincidences per second, with a measurement time per setting of 2 h. The fidelity of the state was measured to be 0.9947 ± 0.0009. The observed success probability $\mathcal{R}$ is 0.9748 ± 0.0001, which is close to the ideal maximum value of 1, thus showing a large advantage due to entanglement.

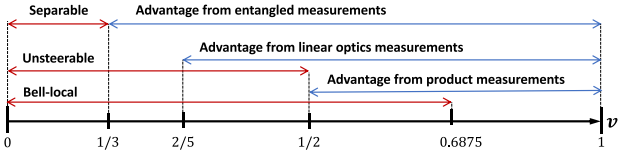

FIG. 3. Nonlocal properties (red) and quantum communication advantages (blue) of the two-qubit isotropic state. The range for quantum communication advantages from general entangled measurements follows from dense-coding-like protocols [9,10]. The ranges shown for quantum communication advantages with passive-linear-optics measurements and product measurements are established in this work and are upper bounds on the critical visibilities.

VII. DISCUSSION

In this paper we demonstrated theoretically, and confirmed experimentally, that one can obtain quantum communication advantages in a secret-sharing task using weakly entangled unsteerable states while being restricted only to product measurements or entangled measurements compatible with passive linear optics. Figure 3 summarizes the ranges of noise v for which quantum communication advantages are achievable with two-qubit isotropic states and the relation to its nonlocal properties. It remains an open question whether the visibilities can be further reduced both for standard linear-optics measurements and product measurements. Of particular relevance is the investigation of whether product measurements also can generate advantages from highly noisy multiqubit states, as this would pave the way for experiments that go beyond small-scale demonstrations.

ACKNOWLEDGMENTS

A.A.A. and A.T. thank Anthony Martin and Alek Lagarrigue for discussions on an early iteration of the task presented here. This work was supported by the Swedish Research Council, the Wenner-Gren Foundation, and the Knut and Alice Wallenberg Foundation through the Wallenberg Center for Quantum Technology.

APPENDIX A: UNSTEERABILITY OF EXPERIMENTAL STATES

Recall that the isotropic state ρ_v is defined as

$$\rho_v = v\Phi^+ + \frac{(1-v)}{4}\mathbb{1}, \tag{A1}$$

where $\Phi^+ = |\phi^+\rangle\langle\phi^+|$. It is well known that ρ_v is unsteerable for $v \leq 1/2$ and entangled for $v > 1/3$ [37]. The

TABLE I. Half-wave-plate rotation angles (in degrees) and phases for the preparation of the different states.

State	Bob's HWP	Charlie's HWP	Phase plate
$\|\phi_\theta^+\rangle$	0	0	0
$\|\phi_\theta^-\rangle$	45	45	Π
$\|\psi_\theta^+\rangle$	0	45	0
$\|\psi_\theta^-\rangle$	45	0	Π

states prepared experimentally, however, are necessarily not exactly the isotropic states. To exhibit an advantage in the stochastic secret-sharing task from entangled but unsteerable states, it is necessary to verify that the experimentally prepared states, as reconstructed via state tomography, are indeed unsteerable. The same is true for the noisy partially entangled states ρ_v^θ defined as

$$\rho_v^\theta = v|\phi_\theta^+\rangle\langle\phi_\theta^+| + \frac{(1-v)}{4}\mathbb{1}, \tag{A2}$$

where $|\phi_\theta^+\rangle = \cos\theta|00\rangle + \sin\theta|11\rangle$, which were used to show an advantage in the deterministic secret-sharing protocol from unsteerable states.

While two-qubit entanglement can easily be verified by calculating its negativity, verifying unsteerability is more challenging. Here we use a recently developed method [36] that allows one to obtain certificates of unsteerability via linear programming.

In particular, the approach of Nguyen *et al.* [36] computes, for an arbitrary two-qubit state and a given direction of steering (say, from Bob to Charlie or from Charlie to Bob), both upper and lower bounds, $r_{\text{crit}}^{\text{upper}}$ and $r_{\text{crit}}^{\text{lower}}$, respectively, on a "critical radius" r_{crit} satisfying $r_{\text{crit}}^{\text{lower}} < r_{\text{crit}} < r_{\text{crit}}^{\text{upper}}$. They show that a two-qubit state ρ is steerable (in a given direction) if and only if $r_{\text{crit}} < 1$. Thus, by finding $r_{\text{crit}}^{\text{lower}} \geq 1$ for both possible directions of steering, we are guaranteed a state is unsteerable.

TABLE II. Transformation table: the operations $\sigma_X^{x_0}\sigma_Z^{x_1}$ and $\sigma_X^{y_0}\sigma_Z^{y_1}$ that need to be performed by Bob and Charlie, respectively. The expected Bell state that Alice will receive in the ideal case that Bob and Charlie share a noiseless maximally entangled state is shown in the final column.

x_0	x_1	y_0	y_1	Bob	Charlie	Alice's expected state
0	0	0	0	$\mathbb{1}$	$\mathbb{1}$	Φ^+
0	0	1	0	$\mathbb{1}$	σ_X	Ψ^+
0	0	1	1	$\mathbb{1}$	$-i\sigma_Y$	Ψ^-
0	0	0	1	$\mathbb{1}$	σ_Z	Ψ^-
1	0	0	0	σ_X	$\mathbb{1}$	Ψ^-
1	0	1	0	σ_X	σ_X	Φ^+
1	0	1	1	σ_X	$-i\sigma_Y$	Φ^-
1	0	0	1	σ_X	σ_Z	Ψ^-
1	1	0	0	$-i\sigma_Y$	$\mathbb{1}$	Ψ^-
1	1	1	0	$-i\sigma_Y$	σ_X	Ψ^+
1	1	1	1	$-i\sigma_Y$	$-i\sigma_Y$	Φ^+
1	1	0	1	$-i\sigma_Y$	σ_Z	Ψ_+
0	1	0	0	σ_Z	$\mathbb{1}$	Φ^-
0	1	1	0	σ_Z	σ_X	Ψ_-
0	1	1	1	σ_Z	$-i\sigma_Y$	Ψ_+
0	1	0	1	σ_Z	σ_Z	Φ_+

TABLE III. Half-wave-plate rotation angles (in degrees) and phases for the unitaries for Bob's and Charlie's operations.

Unitary	HWP	Phase plate
$\mathbb{1}$	0	Π
σ_X	45	0
$-i\sigma_Y$	0	0
σ_Z	45	Π

The precision of the upper and lower bounds can be increased at the cost of computational time and memory. On a standard desktop computer, using the CPLEX package provided by Nguyen *et al.* [36], we were typically able to obtain, for the experimental states approximating ρ_v, a gap $r_{\text{crit}}^{\text{upper}} - r_{\text{crit}}^{\text{lower}} \approx 0.02$ with a few minutes of computation. This can be reduced by an order of magnitude by allocating somewhat more computational time.

For the tomographically reconstructed density matrices $\tilde{\rho}_v$, for $v = 0.4$ to $v = 0.5$ (with a step size of 0.1), we computed $r_{\text{crit}}^{\text{lower}}$ and found the states to be unsteerable for all values of v except 0.5. However, to ensure that this result is robust (recalling, of course, the experimental error in the description of $\tilde{\rho}_v$) and ensure we choose a state providing a large-enough quantum advantage (which diminishes as v decreases), we chose to perform the experiment with $v = 0.47$.

For this state, we performed a finer analysis of the unsteerability of $\tilde{\rho}_{0.47}$, taking into account the errors in each term of the density matrix. Adopting a conservative approach, we applied the worst-case errors to all subsets of density-matrix elements (up to Hermiticity) before calculating $r_{\text{crit}}^{\text{lower}}$ for the (renormalized) perturbed density matrix. We found that in all cases $r_{\text{crit}}^{\text{lower}} \gtrsim 1.031$ (while for the reconstructed state $\tilde{\rho}_{0.47}$ we found $r_{\text{crit}}^{\text{lower}} \approx 1.055$), showing that the prepared state is clearly unsteerable, even when errors are taken into account.

We likewise performed a similar analysis on the tomographically reconstructed density matrix $\tilde{\rho}_v^{\theta_*}$ for $\theta_* = 0.2356$ and $v = 0.72$. By applying worst-case errors in the same manner, we found that in all cases $r_{\text{crit}}^{\text{lower}} \gtrsim$

TABLE IV. Rotation angles (in degrees) for the HWPs used to implement Alice's projective measurements, for $z = 0$ and $z = 1$.

z	HWP 1	HWP 2
0	0	0
1	22.5	22.5

TABLE V. Theoretical and experimental success probabilities for the partially entangled state $|\phi^+_{\theta_*}\rangle$ (with $\theta_* = 0.2356$), conditioned on z and then averaged to give the overall success probability $\mathcal{S}$.

Parameter	Theoretical	Experimental	Error
$S\,(z=0)$	0.5	0.4975	0.0005
$S\,(z=1)$	0.3635	0.35440	0.00009
$\mathcal{S}$	0.8635	0.8519	0.0002

1.020, while for the reconstructed state $\tilde{\rho}^{\theta_*}_v$ itself we found $r^{\text{lower}}_{\text{crit}} \approx 1.031$. As for the isotropic state, we thus see that the experimentally prepared state is clearly unsteerable, even when errors are taken into account.

APPENDIX B: STATE PREPARATION, TRANSFORMATIONS, AND MEASUREMENTS FOR THE DETERMINISTIC SECRET-SHARING EXPERIMENT

1. State implementation

The setup used generates an entangled $|\phi^+_\theta\rangle = \cos\theta|00\rangle + \sin\theta|11\rangle$ state with a visibility close to 100%. To create this state, we use an HWP to change the power distribution between the horizontally polarized crystal and the vertically polarized crystal. When the angle of this HWP is 0°, only the horizontally polarized crystal is pumped, and when the angle of the HWP is 90°, only the vertically polarized crystal is pumped. When the angle is 45°, the prepared state is $|\phi^+\rangle$. We have to select the correct angle (θ) to prepare the desired state. To create the maximally mixed state $\mathbb{1}/4$, we randomly switch between $|\phi^+_\theta\rangle$, $|\phi^-_\theta\rangle = \sin\theta|00\rangle - \cos\theta|11\rangle$, $|\psi^+_\theta\rangle = \cos\theta|01\rangle + \sin\theta|10\rangle$, and $|\psi^-_\theta\rangle = \sin\theta|01\rangle - \cos\theta|10\rangle$. Indeed, these states form an orthonormal basis.

We can thereby generate ρ^θ_v for any value of v by choosing correctly the weights with which we randomly change $|\phi^+_\theta\rangle$ to one of the other states. The switching between these different states is done with the help of two half-wave plates and a phase plate; see Fig. 2.

These plates are motorized and switched randomly (with the desired probability) from one state to another every second. The number of coincidences being less than one per second, the result is switching from one state to another randomly and independently between each pair of successive coincidences. The angles allowing one to pass from one state to another are given in Table I.

TABLE VI. Theoretical and experimental success probabilities for $\rho^{\theta_*}_v$ with $v = 0.72$, conditioned on z and then averaged to give the overall success probability $\mathcal{S}$.

Parameter	Theoretical	Experimental	Error
$S\,(z=0)$	0.43	0.43	0.001
$S\,(z=1)$	0.3317	0.327	0.002
$\mathcal{S}$	0.7617	0.757	0.001

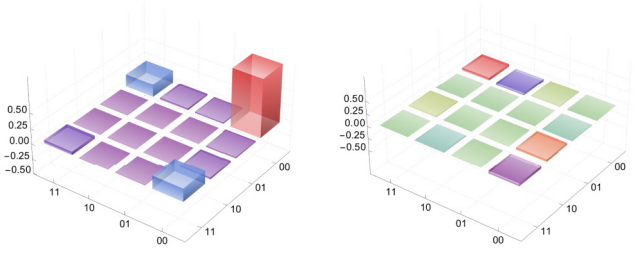

FIG. 4. State tomography of $\rho^{\theta_*}_v$ for $v = 1$; the real part of the density matrix is shown on the left, and the imaginary part on the right.

APPENDIX C: BOB'S AND CHARLIE'S ROTATIONS

As described in the main text, on inputs $x = (x_0, x_1) \in \{0,1\}^2$ and $y = (y_0, y_1) \in \{0,1\}^2$, Bob and Charlie apply the unitaries $U^B_x = \sigma_X^{y_0}\sigma_Z^{y_1}$ and $U^C_y = \sigma_X^{y_0}\sigma_Z^{y_1}$, respectively.

Table II summarizes explicitly the operations that Bob and Charlie must perform for inputs x and y, as well as the Bell state expected to be received by Alice in the ideal case (assuming Bob and Charlie share a Φ^+ state). The settings to be applied to achieve each of the four different possible rotations are given in Table III.

1. Alice's measurements

Depending on her setting $z \in \{0,1\}$, Alice performs a projective measurement in the diagonal basis or in the H-V basis. To make these measurements, she uses two HWPs placed before the input ports of each PBS (see Fig. 2). The angles of these HWPs are given in Table IV.

APPENDIX D: EXPERIMENTAL RESULTS AND ERROR ESTIMATION FOR THE DETERMINISTIC SECRET-SHARING EXPERIMENT

Tables V and VI list our experimental results along with the theoretical success rates $\mathcal{S}$.

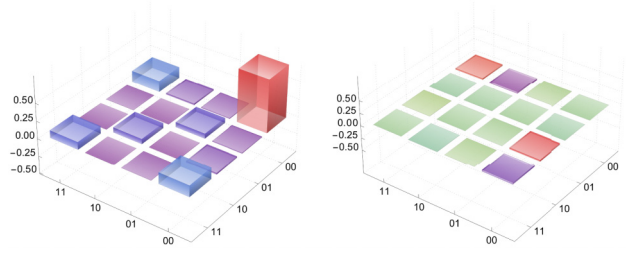

FIG. 5. State tomography of $\rho^{\theta_*}_v$ for $v = 0.72$; the real part of the density matrix is shown on the left and the imaginary part is shown on the right.

TABLE VII. Fidelity of measured states with the ideal state $\rho_v^{\theta_*}$ for $v = 0.72$ and $v = 1$.

Visibility v	Fidelity with $\rho_v^{\theta_*}$	Error
0.72	0.9965	0.0007
1.00	0.990	0.001

The errors were calculated with the same method as for the stochastic secret-sharing experiment.

APPENDIX E: DENSITY-MATRIX TOMOGRAPHY FOR THE DETERMINISTIC SECRET-SHARING EXPERIMENT

To ensure that the prepared state is the desired one, a tomography measurement is performed for a perfect $|\phi_{\theta_*}^+\rangle$ state and for the noisy states $\rho_v^{\theta_*}$ with a visibility v of 0.72 (and with $\theta_* = 0.2356$), which are the two states for which the experimental demonstration of the protocol was conducted. The reconstructed density matrices are shown in Figs. 4 and 5, respectively.

The fidelity of each state obtained during the tomography with the ideal state $\rho_v^{\theta_*}$ was found to be above 0.99. Table VII gives the fidelity for each of these states.

APPENDIX F: STATE PREPARATION, TRANSFORMATIONS, AND MEASUREMENTS FOR THE STOCHASTIC SECRET-SHARING EXPERIMENT

1. State implementation

The setup used generates an entangled Φ^+ state with a visibility close to 100%. To generate an isotropic state ρ_v (A1), this state needs to be mixed with probability $(1 - v)$ with the maximally mixed state $\mathbb{1}/4$. We implement the maximally mixed state by randomly switching between the four Bell states, $\Phi^{\pm}, \Psi^{\pm}$, using the fact that $\mathbb{1}/4 = 1/4(\Phi^+ + \Phi^- + \Psi^+ + \Psi^-)$. We can thereby generate ρ_v for any value of v by choosing correctly the weights with which we randomly change Φ^+ to one of the other Bell states.

The switching between these different states is done with the help of one half-wave plate and a phase plate; see Fig. 2.

TABLE VIII. Half-wave-plate rotation angles (in degrees) and phases for the preparation of the different Bell states.

State	HWP	Phase plate
Φ^+	0	0
Φ^-	0	Π
Ψ^+	45	0
Ψ^-	45	Π

TABLE IX. Rotation angles (in degrees) for the HWPs used to implement Alice's partial Bell-state measurements, for $z = 0$ and $z = 1$.

z	HWP 1	HWP 2	HWP 3
0	0	45	0
1	0	22.5	22.5

These plates are motorized and switched randomly (with the desired probability) from one state to another every second. The number of coincidences being less than one per second, the result is switching from one Bell state to another randomly and independently between each pair of successive coincidences. The angles allowing one to pass from one state to another are given in Table VIII.

2. Bob's and Charlie's rotations

Bob's and Charlie's rotations are the same as in the stochastic secret-sharing experiment; see Appendix C.

3. Alice's measurements

Depending on her setting $z \in \{0, 1\}$, Alice performs one of the three-outcome partial Bell measurements $\{\Psi^+, \Psi^-, \Phi^+ + \Phi^-\}$ or $\{\Phi^-, \Psi^-, \Phi^+ + \Psi^+\}$ and obtains an outcome $c \in \{0, 1, \perp\}$. To make these measurements, she uses three HWPs , with the first two placed before one of the input ports of the PBS, and last one placed before the other input port (see Fig. 2). The angles of these HWPs are given in Table IX.

APPENDIX G: EXPERIMENTAL RESULTS AND ERROR ESTIMATION FOR THE ISOTROPIC STATES ρ_v

Tables X and XI list our experimental results along with the theoretical success rates $\mathcal{R}$ with the related errors.

To calculate these errors, following Ref. [38] we consider errors originating from the measurement side only. To reduce experimental errors in the measurements, we used computer-controlled high-precision motorized rotation stages for Bob, Charlie, and the generation of Werner states to set the orientation of the wave plates with a repeatably high precision of 0.02°. The use of different settings (x, y) induces a systematic error, which we estimate using

TABLE X. Theoretical and experimental success rate for the maximally entangled state Φ^+, conditioned on z and then averaged to give the overall success rate $\mathcal{R}$.

Parameter	Theoretical	Experimental	Error
R_{control} $(z = 0)$	1	0.9900	0.0002
R_{secret} $(z = 0)$	1	0.9811	0.0003
R_{control} $(z = 1)$	1	0.9795	0.0002
R_{secret} $(z = 1)$	1	0.9485	0.0003
$\mathcal{R}$	1	0.9748	0.0001

TABLE XI. Theoretical and experimental success rates for the isotropic state ρ_v with $v = 0.47$, conditioned on z and then averaged to give the overall success rate $\mathcal{R}$.

Parameter	Theoretical	Experimental	Error
R_{control} $(z = 0)$	0.735	0.7238	0.0007
R_{secret} $(z = 0)$	0.6025	0.6086	0.0009
R_{control} $(z = 1)$	0.735	0.6613	0.0007
R_{secret} $(z = 1)$	0.603	0.6161	0.001
$\mathcal{R}$	0.66875	0.6524	0.0004

Monte Carlo simulation. We assume that the wave plates' setting errors are normally distributed with a standard deviation of 0.02°. Alice's wave plates are not motorized. To reduce systematic errors in the angle settings, all settings for $z = 0$ are measured and then all settings for $z = 1$ are measured, so the results are initially presented separately for each case. We estimate the accuracy of the angles of these WPs to be 0.5°. This, together with the Poissonian error in photon-counting statistics, constitutes the final error reported here. Because of inefficiency of the single-photon detectors, the photons are detected randomly and their counting is Poissonian. To decrease Poissonian counting error, we chose for $v = 1$ a measurement time of 2 h for every setting and collected approximately 93×10^6 events. To guarantee that both parties receive single qubits, we worked at a low rate (approximately 800 coincidences per second) to suppress higher-order coincidences to almost 0.9 per second. For $v = 0.47$, we collected around one million two-photon coincidences, and the low rate renders the higher-order coincidences completely negligible.

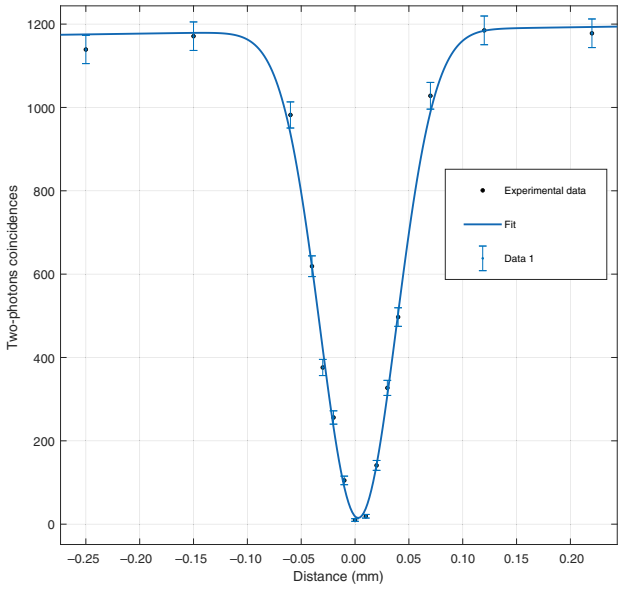

FIG. 6. Two-fold Hong-Ou-Mandel dip. The plot displays the twofold photon-counting coincidence versus the delay (the path difference between the two arms). The error bars indicate the Poissonian photon-counting error statistics. The data are fitted with a Gaussian curve.

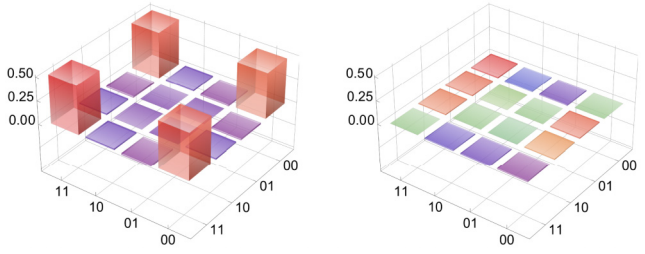

FIG. 7. State tomography of ρ_v for $v = 1$; the real part of the density matrix is shown on the left and the imaginary part is shown on the right.

APPENDIX H: TWOFOLD HONG-OU-MANDEL DIP VISIBILITY

Bell-state measurements are implemented through two-photon interference, using PBSs and HWPs set at 22.5°. The photons are detected by Si avalanche photodiodes and the coincidences are registered with an eight-channel multifold coincidence-counting unit. This Bell analyzer consists of coherent interference at a PBS. To achieve the necessary indistinguishability of the photons, due to their arrival times, we adjusted the path length of one of the photons using a delay line [39]. In Fig. 6, the coincidence between the detectors versus the delay path length is shown. The zero delay corresponds to a maximal overlap (maximum indistinguishability). The interfering photons bunch (i.e., they both exit in the same output arm of the PBS), causing the coincidences to vanish. The measured visibility of the twofold Hong-Ou-Mandel dip is $(99.2 \pm 0.6)\%$, with a coincidence rate outside the dip of around 0.9224 coincidences per second, identical to the rate at which we performed the experiment for $v = 0.47$.

APPENDIX I: DENSITY-MATRIX TOMOGRAPHY FOR THE STOCHASTIC SECRET-SHARING EXPERIMENT

To ensure that the prepared state is the desired one, a tomography measurement is performed for a perfect Φ^+ state and for isotropic states ρ_v with a visibility v between

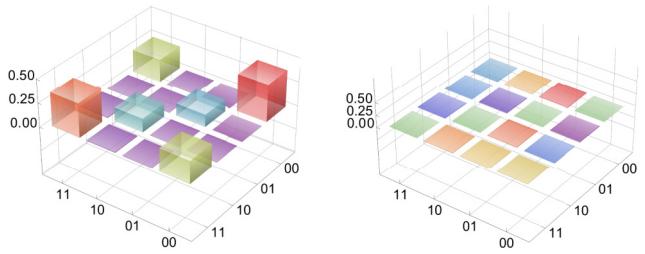

FIG. 8. State tomography of ρ_v for $v = 0.47$; the real part of the density matrix is shown on the left and the imaginary part is shown on the right.

TABLE XII. Fidelity of each measured state with the ideal isotropic state ρ_v.

Visibility v	Fidelity with ρ_v	Error
0.4	0.9982	0.0004
0.41	0.9982	0.0004
0.42	0.9983	0.0004
0.43	0.9983	0.0004
0.44	0.9983	0.0004
0.45	0.9983	0.0004
0.46	0.9983	0.0004
0.47	0.9983	0.0004
0.48	0.9983	0.0004
0.49	0.9983	0.0004
0.50	0.9983	0.0004
1.00	0.9947	0.0009

0.4 and 0.5. The reconstructed density matrices obtained for the cases of $v = 1$ (i.e., the ideal case of $\rho_1 = \Phi^+$) and $v = 0.47$, which are the two states for which the experimental demonstration of the protocol was conducted, are presented in Figs. 7 and 8, respectively.

The fidelity of each state obtained during the tomography with the ideal isotropic state ρ_v was found to be between 0.9947 and 0.9983. Table XII gives the fidelity for each of these states.

[1] R. Cleve and H. Buhrman, Substituting quantum entanglement for communication, Phys. Rev. A **56**, 1201 (1997).

[2] Č. Brukner, M. Żukowski, J.-W. Pan, and A. Zeilinger, Bell's inequalities and quantum communication complexity, Phys. Rev. Lett. **92**, 127901 (2004).

[3] T. S. Cubitt, D. Leung, W. Matthews, and A. Winter, Improving zero-error classical communication with entanglement, Phys. Rev. Lett. **104**, 230503 (2010).

[4] N. Brunner and N. Linden, Connection between Bell nonlocality and Bayesian game theory, Nat. Commun. **4**, 2057 (2013).

[5] A. Tavakoli and M. Żukowski, Higher-dimensional communication complexity problems: Classical protocols versus quantum ones based on Bell's theorem or prepare-transmit-measure schemes, Phys. Rev. A **95**, 042305 (2017).

[6] A. Tavakoli, M. Żukowski, and Č. Brukner, Does violation of a Bell inequality always imply quantum advantage in a communication complexity problem?, Quantum **4**, 316 (2020).

[7] J. Pauwels, S. Pironio, E. Z. Cruzeiro, and A. Tavakoli, Adaptive advantage in entanglement-assisted communications, Phys. Rev. Lett. **129**, 120504 (2022).

[8] C. H. Bennett and S. J. Wiesner, Communication via one- and two-particle operators on Einstein-Podolsky-Rosen states, Phys. Rev. Lett. **69**, 2881 (1992).

[9] A. Tavakoli, A. A. Abbott, M.-O. Renou, N. Gisin, and N. Brunner, Semi-device-independent characterisation of multipartite entangled states and measurements, Phys. Rev. A **98**, 052333 (2018).

[10] G. Moreno, R. Nery, C. de Gois, R. Rabelo, and R. Chaves, Semi-device-independent certification of entanglement in superdense coding, Phys. Rev. A **103**, 022426 (2021).

[11] M. J. Renner, Compatibility of all noisy qubit observables, arXiv:2309.12290 [quant-ph] (2023).

[12] Y. Zhang and E. Chitambar, Exact steering bound for two-qubit Werner states, arXiv:2309.09960 [quant-ph] (2023).

[13] S. Designolle, G. Iommazzo, M. Besançon, S. Knebel, P. Gelß, and S. Pokutta, Improved local models and new Bell inequalities via Frank-Wolfe algorithms, Phys. Rev. Research **5**, 043059 (2023).

[14] N. Lütkenhaus, J. Calsamiglia, and K.-A. Suominen, Bell measurements for teleportation, Phys. Rev. A **59**, 3295 (1999).

[15] K. Mattle, H. Weinfurter, P. G. Kwiat, and A. Zeilinger, Dense coding in experimental quantum communication, Phys. Rev. Lett. **76**, 4656 (1996).

[16] X. Li, Q. Pan, J. Jing, J. Zhang, C. Xie, and K. Peng, Quantum dense coding exploiting a bright Einstein-Podolsky-Rosen beam, Phys. Rev. Lett. **88**, 047904 (2002).

[17] J. T. Barreiro, T.-C. Wei, and P. G. Kwiat, Beating the channel capacity limit for linear photonic superdense coding, Nat. Phys. **4**, 282 (2008).

[18] B. P. Williams, R. J. Sadlier, and T. S. Humble, Superdense coding over optical fiber links with complete Bell-state measurements, Phys. Rev. Lett. **118**, 050501 (2017).

[19] X.-M. Hu, Y. Guo, B.-H. Liu, Y.-F. Huang, C.-F. Li, and G.-C. Guo, Beating the channel capacity limit for superdense coding with entangled ququarts, Sci. Adv. **4**, eaat9304 (2018).

[20] A. Piveteau, J. Pauwels, E. Håkansson, S. Muhammad, M. Bourennane, and A. Tavakoli, Entanglement-assisted quantum communication with simple measurements, Nat. Commun. **13**, 7878 (2022).

[21] G. R. Blakley, in *Proceedings of the 1979 AFIPS National Computer Conference* (AFIPS Press, Monval, NJ, USA, 1979), p. 313.

[22] A. Shamir, How to share a secret, Commun. ACM **22**, 612 (1979).

[23] M. Hillery, V. Bužek, and A. Berthiaume, Quantum secret sharing, Phys. Rev. A **59**, 1829 (1999).

[24] A. Karlsson, M. Koashi, and N. Imoto, Quantum entanglement for secret sharing and secret splitting, Phys. Rev. A **59**, 162 (1999).

[25] G.-P. Guo and G.-C. Guo, Quantum secret sharing without entanglement, Phys. Lett. A **310**, 247 (2003).

[26] A. Tavakoli, I. Herbauts, M. Żukowski, and M. Bourennane, Secret sharing with a single d-level quantum system, Phys. Rev. A **92**, 030302 (2015).

[27] V. Karimipour and M. Asoudeh, Quantum secret sharing and random hopping: Using single states instead of entanglement, Phys. Rev. A **92**, 030301 (2015).

[28] H. Weinfurter, Experimental Bell-state analysis, Europhys. Lett. **25**, 559 (1994).

[29] S. L. Braunstein and A. Mann, Measurement of the Bell operator and quantum teleportation, Phys. Rev. A **51**, R1727 (1995).

[30] M. Navascués and T. Vértesi, Bounding the set of finite dimensional quantum correlations, Phys. Rev. Lett. **115**, 020501 (2015).

[31] Specifically, we used what would, in standard terminology, be called the "$1 + AB + AC + ABC$" level, leading to a moment matrix of size 109.

[32] M. Fillettaz, F. Hirsch, S. Designolle, and N. Brunner, Algorithmic construction of local models for entangled quantum states: Optimization for two-qubit states, Phys. Rev. A **98**, 022115 (2018).

[33] J. Calsamiglia and N. Lütkenhaus, Maximum efficiency of a linear-optical Bell-state analyzer, Appl. Phys. B **72**, 67 (2001).

[34] Note that $\mathcal{R}$ is invariant under (i) simultaneous bit flip of x_0 and y_0, (ii) simultaneous bit flips of x_1 and y_1, and (iii) simultaneous swaps $x_0 \leftrightarrow x_1$ and $y_0 \leftrightarrow y_1$.

[35] A. Tavakoli, D. Rosset, and M.-O. Renou, Enabling computation of correlation bounds for finite-dimensional quantum systems via symmetrization, Phys. Rev. Lett. **122**, 070501 (2019).

[36] H. C. Nguyen, H.-V. Nguyen, and O. Gühne, Geometry of Einstein-Podolsky-Rosen correlations, Phys. Rev. Lett. **122**, 240401 (2019).

[37] H. M. Wiseman, S. J. Jones, and A. C. Doherty, Steering, entanglement, nonlocality, and the Einstein-Podolsky-Rosen paradox, Phys. Rev. Lett. **98**, 140402 (2007).

[38] H. Anwer, S. Muhammad, W. Cherifi, N. Miklin, A. Tavakoli, and M. Bourennane, Experimental characterization of unsharp qubit observables and sequential measurement incompatibility via quantum random access codes, Phys. Rev. Lett. **125**, 080403 (2020).

[39] C. K. Hong, Z. Y. Ou, and L. Mandel, Measurement of subpicosecond time intervals between two photons by interference, Phys. Rev. Lett. **59**, 2044 (1987).